

TECHNIQUE

10.1002/2013JA019641

Key Points:

- Taylor microscale is important in turbulence
- Measurement is hindered by finite time resolution data
- Technique given here improves estimates

Correspondence to:

W. H. Matthaeus,  
whm@udel.edu

Citation:

Chuychai, P., J. M. Weygand, W. H. Matthaeus, S. Dasso, C. W. Smith, and M. G. Kivelson (2014), Technique for measuring and correcting the Taylor microscale, *J. Geophys. Res. Space Physics*, 119, 4256–4265, doi:10.1002/2013JA019641.

Received 21 NOV 2013

Accepted 4 MAY 2014

Accepted article online 8 MAY 2014

Published online 6 JUN 2014

Technique for measuring and correcting the Taylor microscale

P. Chuychai<sup>1,2</sup>, J. M. Weygand<sup>3</sup>, W. H. Matthaeus<sup>4</sup>, S. Dasso<sup>5</sup>, C. W. Smith<sup>6</sup>, and M. G. Kivelson<sup>3</sup>

<sup>1</sup>School of Science, Mae Fah Luang University, Chiang Rai, Thailand, <sup>2</sup>Thailand Center of Excellence in Physics, CHE, Ministry of Education, Bangkok, Thailand, <sup>3</sup>Institute for Geophysics and Planetary Physics, University of California, Los Angeles, California, USA, <sup>4</sup>Bartol Research Institute, Department of Physics and Astronomy, University of Delaware, Newark, Delaware, USA, <sup>5</sup>Instituto de Astronomia y Fisica del Espacio (CONICET-UBA) and Departamento de Fisica (FCEN-UBA), Buenos Aires, Argentina, <sup>6</sup>Space Science Center, University of New Hampshire, Durham, New Hampshire, USA

**Abstract** We discuss and develop methods to estimate and refine measurements of the Taylor microscale from discrete data sets. To study how well a method works, we construct a time series of discrete data with a known power spectrum and Taylor scale, but with various truncations of the resolution that eliminate higher frequencies in a controlled fashion. We compute the second-order structure function and correlation function, assuming that the unresolved dissipation range spectrum has various values of spectral index. A series of Taylor scale estimates are obtained from parabolic fits to subsets of the correlation function data, and these are extrapolated to the limit of zero separation. The error in this procedure, for finite time resolution sampling, depends on the spectral index in the dissipation range. When the spectral form is known, we can compute a correction factor that improves the estimate of the Taylor microscale value determined from the extrapolation method and band-limited data. Application of this technique to spacecraft observations of solar wind fluctuations is illustrated.

1. Introduction

The motivation of this study comes from recent efforts to measure the Taylor microscale in solar wind turbulence calculated using multispacecraft techniques [Matthaeus *et al.*, 2005; Weygand *et al.*, 2007, 2009, 2010, 2011; Gurgiolo *et al.*, 2013]. The Taylor scale is related to the second derivatives of the data [Batchelor, 1970] (also see below); therefore, it is inherently sensitive to the high-frequency spectral content of the signal. Of course, for idealized time-continuous infinite precision data, the Taylor scale may be computed. Likewise, when very high cadence measurements are available [e.g., Alexandrova *et al.*, 2009; Sahraoui *et al.*, 2009], and the spectrum is steep enough (see below), it may be possible to unambiguously determine the Taylor scale. However, for available data sets with finite time cadence, the values of the Taylor scale obtained by a straightforward evaluation may be sensitive to the data resolution, as the correct value may depend on the physical signal above the sampling Nyquist frequency.

The objective of this study is to understand the accuracy of the Taylor scale estimates using finite resolution data sets, in which the high-frequency spectra may or may not be well known. We develop a method to improve these estimates based on the spectrum of the unresolved data, which can be used when estimates of the high-frequency spectrum of the signal are available in some way, whether it be observations, theory, or an informed guess. Although the main purpose here is to discuss measurement issues, the physical significance of the Taylor scale will be reviewed briefly in section 2.

In a system such as the solar wind, the Taylor microscale can be estimated from single spacecraft analyses. Within the context of the Taylor [1938] frozen-in flow approximation, time *t* separation is converted to spatial *x* separation using the relation  $x = V_{sw} \times t$ . In the latter case, instead of working in the spatial domain, the curvature of the two time correlation near the origin can be estimated. Frozen-in flow is a standard approximation in solar wind observational analysis and in wind tunnels. Dasso *et al.* [2008] demonstrates the validity of this approximation in the solar wind by comparing values determined from single spacecraft and multispacecraft analysis. With this background in mind, one can define the Taylor microscale ( $\lambda_T$ ) by

$$\frac{1}{\lambda_T} = \sqrt{\frac{\langle (\frac{\partial F}{\partial x})^2 \rangle}{\langle F^2 \rangle}} \rightarrow \frac{1}{V_{sw} \tau_{TS}} = \frac{1}{V_{sw}} \sqrt{\frac{\langle (\frac{\partial F}{\partial t})^2 \rangle}{\langle F^2 \rangle}}, \tag{1}$$

where  $F$  is the function of interest such as the velocity or magnetic field fluctuations. For generality and simplicity, here we will discuss methods for arriving at improved estimates of the Taylor scale under the assumption that the problem of interest is in the time domain or that frozen-in flow is valid. Therefore, the discussion will center on the procedure to extract  $\tau_{TS}$  from a time series  $F(t)$ . We will employ a model spectrum in which the inertial range terminates by steepening at a “dissipation scale” (Kolmogorov scale) or its equivalent in the time domain  $\tau_d$ , which is the equivalent sweeping time of the dissipation length scale past the detector. Thus, in the present paper the term dissipation scale implies only the scale at which the power law cascade range terminates, generally leading to a steeper spectrum. This familiar terminology is used in a purely kinematic sense, without regard for whether this steepening is due to dissipation, dispersion, or some other effect.

Focusing on the time domain, the Taylor microscale can be also viewed as the radius of curvature at the origin of the autocorrelation function

$$R(\tau) = \langle F(t)F(t + \tau) \rangle. \quad (2)$$

From a small  $\tau$  expansion, and using  $R(\tau) = R(-\tau)$ , a requirement of time stationarity, the autocorrelation function near the origin, can be determined by

$$R(\tau) \approx 1 - \frac{\tau^2}{2\tau_{TS}^2} + \dots \quad (3)$$

Therefore, one way to obtain the Taylor microscale from measurements is to fit  $R(\tau)$  at the origin. However, sometimes the observation data do not have sufficient time resolution near the origin to perform an adequate parabolic fit. This is due to the fact that for many reasonable spectra, the quadratic behavior suggested in equation (3) is not apparent until the correlation function is sampled at scales  $\tau < \tau_d$ . We will study the expected effects on Taylor scale determination using a designed function  $F(t)$  that is intentionally under-sampled but which is extracted from a signal that has better time resolution and a known spectral index in the dissipation range. This is a useful approach to develop a procedure that reliably determines the Taylor microscale. To develop this technique we construct the time data series based on a specified spectrum. With varying resolution synthetic data, we obtain empirical values of the Taylor microscale and compare with the known “exact” values. We find that it is possible to define a multiplicative correction factor that allows us in some circumstances to adjust and improve the measured Taylor scale based on assumptions about the spectrum of the unresolved high-cadence data.

Before turning to the main content of the paper, we digress briefly concerning the physical significance of the Taylor scale, both in hydrodynamics [Batchelor, 1970] and in the case of collisionless plasma such as the solar wind. In isotropic hydrodynamic turbulence, the Taylor scale may be defined as the radius of curvature at the origin of the two-point velocity ( $\mathbf{v}$ ) correlation  $R(r) = \langle \mathbf{v}(0) \cdot \mathbf{v}(\mathbf{r}) \rangle$ ; that is,  $\lambda_T^2 = R(0)/R''(0)$  or equally well as the length associated with the mean square curl of the velocity (the vorticity),  $\lambda_T^2 = \frac{\langle |\mathbf{v}|^2 \rangle}{\langle |\nabla \times \mathbf{v}|^2 \rangle}$ . For viscous ( $\nu$ ) dissipation in an incompressible medium, the Taylor scale is also related to dissipation, in that (for suitable boundary conditions),  $\frac{d\langle |\mathbf{v}|^2 \rangle}{dt} = -\nu \lambda_T^{-2} \langle |\mathbf{v}|^2 \rangle$ . In this sense the Taylor scale is the “equivalent dissipation scale,” in that, any instant of time, the dissipation rate is the same as if all the energy were at the Taylor scale. In older turbulence texts [Hinze, 1975] the Taylor scale is sometimes designated simply as “the dissipation scale.” However, in more current terminology the latter is usually reserved for the Kolmogorov scale  $\eta$  which signifies the scale (or wave number  $1/\eta$ ) at which the power law inertial range terminates and beyond which lies the dissipation range. For high Reynolds number  $R$  and correlation scale  $L$ , in hydrodynamics, the Taylor scale is  $\lambda_T = L/\sqrt{R}$ , while  $\eta = L/R^{3/4}$ . Therefore,  $\lambda_T/\eta = R^{1/4}$ , and the two become well separated at very large  $R$ . For plasmas the dynamical status of both the Taylor scale and the Kolmogorov scale becomes ambiguous [see, e.g., Matthaeus et al., 2008]. The mechanism of dissipation is not well understood for collisionless plasma and may vary in different parameter regimes. Thus,  $\lambda_T$  cannot be interpreted as connected with the length scale or rate of energy dissipation. Likewise, the termination of the inertial range may not be associated with dissipation, as the onset of kinetic dispersive waves may also be influential. Nevertheless, it is convenient to maintain the kinematic definitions of Taylor scale and “dissipation scale,” related respectively to the second derivative of the correlation function at the origin and the termination of the inertial range. In the remainder of the paper we adopt the kinematic meaning of  $\lambda_T$  and the dissipation scale, as well as their time domain counterparts, to be defined below.

## 2. Generating Discrete Data With a Known Taylor Scale

To develop our method, we use synthetic data generated using a known spectrum and then employ a typical methodology to evaluate the Taylor microscale. The spectrum is constructed with inertial and dissipation ranges that have been independently controlled and have generally different power law indices. To be specific, we let the inertial range have a spectral index of  $-5/3$ , while the dissipation range has an adjustable spectral index  $q$ . The particular functional form of the spectrum is

$$P(f) = \begin{cases} \frac{C}{[1+(f\tau_0)^2]^{5/6}}, & \text{where } f_{\min} < f \leq f_d \\ \frac{C}{[1+(f_d\tau_0)^2]^{5/6}} \left(\frac{f_d}{f}\right)^q, & \text{where } f_d < f \leq f_e \\ 0, & \text{where } f_e < f \leq f_{\max}, \end{cases} \quad (4)$$

where  $q < 0$ . The reasons for these choices are as follows: First, the flat spectral region at very low frequencies  $f\tau_0 \ll 1$  is designed to make the signal time stationary. This is unrealistic for the solar wind, which has very low frequency components due to, e.g., solar rotation and solar cycle [see, e.g., *Matthaeus and Goldstein, 1982*]. However, we are not concerned with very low frequency effects here. Second, the inertial range with Kolmogorov spectral index of  $\sim 5/3$  is found for higher frequencies, at  $f\tau_0 > 1$ . Third, there is a discontinuous jump at the top of the inertial range at frequency  $f_d$ , the slope steepening from  $-5/3$  to  $-|q|$ , in qualitative accord with observations [*Leamon et al., 1998; Hamilton et al., 2008; Alexandrova et al., 2009; Sahraoui et al., 2009*]. Finally, at high frequencies  $f > f_e$  we set the spectrum to zero, for numerical rather than physical reasons, to provide a very smooth trigonometric interpolation of the signal at the grid scale.

Adopting illustrative values that are representative of the solar wind at 1 AU, we assume that the spectrum starts from  $f_{\min} = 1.22 \times 10^{-5}$  Hz and is flat until  $f_0 = 1/\tau_0 = 3.906 \times 10^{-4}$  Hz, a “bendover” frequency often associated with the correlation scale or coherence time. Thereafter, the spectrum has an inertial range with a  $5/3$  power law index, until a second breakpoint is encountered at  $f_d = 1/\tau_d = 0.4$  Hz. For historical reasons, this breakpoint, which terminates the power law MHD-scale inertial range, is often referred to as the dissipation scale [*Leamon et al., 1998*], although it is also possible that it characterizes dispersion in addition to dissipation [*Gary and Borovsky, 2004*]. In the hydrodynamic case the eddy turnover time and viscous dissipation time scales become equal at the dissipation scale. However, for the solar wind or other low-collisionality astrophysical plasmas, it is unclear whether the fluctuations become critically damped at the breakpoint/dissipation scale. For example, the inertial range is typically found to terminate near the proton gyroscals, and while some dissipation may occur at such scales, further kinetic plasma dynamics may transfer energy to higher frequencies until much smaller electron scales are encountered [*Alexandrova et al., 2009; Sahraoui et al., 2009*]. It has been argued that a substantial fraction of actual dissipation may occur due to electrons. In any case the scale  $f_d$  corresponds to the onset of kinetic processes and the end of the Kolmogorov-like inertial range. It is, however, the kinematic properties of the spectrum that come into play in the current study, rather than the dynamical origin of the spectral forms.

In our model beyond the breakpoint  $f_d$ , we extend the dissipation range with power law index  $q$  until  $f_e = 16.0$  Hz. This may be considered in the solar wind application to be associated with the electron dissipation scale. The spectrum cuts off completely at  $f_{\max} = 25.6$  Hz. To decide upon these numerical values, here we assume that the dissipation scale and electron dissipation scale correspond to the proton and electron inertial scales, respectively. Thus, we set  $f_e/f_d = 40$  to be consistent with the ratio of electron and proton inertial scales in MHD, which is about  $\sqrt{m_p/m_e} = 42.9$  [see, e.g., *Sahraoui et al., 2009*].

Once we have specified the spectrum, we generate realizations of the signal in the frequency domain,  $F(f)$ , as

$$F(f) = \sqrt{P(f)} \exp [i\phi] \quad (5)$$

where  $\phi$  is a random phase. Then a fast Fourier transform is used to convert the function  $F(f)$  into the real-time domain. In the simulations reported here, we employ this approach to obtain  $2^{22}$  data points for the time series.

**Table 1.** Showing Index  $q$  Which We Vary for Each Case and Their Taylor Scales When We Fix the Dissipation Scale ( $\tau_d = 2.5$  s)

case	$\tau_{TS}^{expect}$ [s]	$\tau_{TS}^{expect}$ [ $\tau_d$ ]
$q = -\infty$	6.569	2.63
$q = -5$	5.097	2.04
$q = -4$	4.368	1.75
$q = -3$	2.869	1.15
$q = -7/3$	1.607	0.64
$q = -2$	1.095	0.44
$q = -1$	0.095	0.028

We next compute the Taylor microscale from the data set we generated by employing the definition equation (1). In Table 1, we give the Taylor microscale values for a range of dissipation scale indices  $q$  corresponding to the generic power spectrum shown in Figure 1. (Note that the spectra are given here as Fourier amplitudes squared, which can easily be converted to power spectral density.) We will treat these expected values of the Taylor microscale as the true or exact Taylor microscale values for the synthetic time series data. To examine and test our extrapolation method, we use only one eighth of the original data. The purpose of defining this subset is that any consistent method will provide good (and even convergent) values of  $\tau_{TS}$  when the time resolution  $\Delta t$  of the estimates is very fine, i.e., the spectral cutoff is resolved

and  $\Delta t f_{max} < 1/2$ . However, our motivation is to obtain reasonably accurate values of  $\tau_{TS}$  when the effective resolution of the data sampling is adjusted so that we are not in this asymptotic regime—a circumstance that is more likely to be realized in practice when analyzing spacecraft data.

With the subset of our discrete time series, we compute the second-order structure function. This can be used to obtain an estimate of the correlation function. We then determine the radius of curvature from correlation function and an estimate of the Taylor microscale. In the following section, we will demonstrate an extrapolation technique [Weygand *et al.*, 2007, 2009, 2010, 2011] to estimate Taylor microscale from a series of parabolic fits of the correlation function near the origin. The details of the method we use are given in the following subsections.

### 2.1. Correlation Function and Structure Function

In estimating the correlation function from many samples of data, it is useful to employ the normalized correlation function

$$\hat{R} = \frac{R}{\langle [F(t)]^2 \rangle}. \tag{6}$$

This reduces errors associated with variability of the variance, i.e., the fluctuation energy. Almost the same information is contained in the second-order structure function  $S_2$ , given by

$$S_2(\tau) = \langle [F(t + \tau) - F(t)]^2 \rangle. \tag{7}$$

In fact,

$$\hat{R}(\tau) = 1 - \frac{S_2(\tau)}{2\langle [F(t)]^2 \rangle}. \tag{8}$$

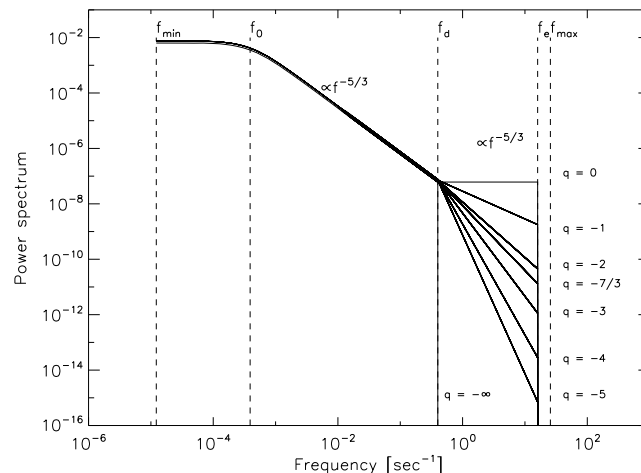


**Figure 1.** The power spectrum for a number of values of  $q$  in the dissipation range.

Figure 2 shows the structure functions for various dissipation range indices  $q$  that we generated as described in section 2. Note that values of dissipation range spectral index in the range  $-5/3 < q < -1$  are pathological in that the implied “dissipation range” has either the same or shallower spectral power law than that found in the inertial range. These values are included only for illustration. As  $q$  is varied, several regimes are seen:

1. For  $\tau \gg \tau_d$ , which is associated with the inertial range ( $f^{-5/3}$ ) in Fourier space, one expects to find  $S_2 \propto \tau^{2/3}$ .
2. For  $\tau \ll \tau_d$  and with  $q = -5$  and  $-4$ , one finds (see Figure 2) that  $S_2 \propto \tau^2$ .

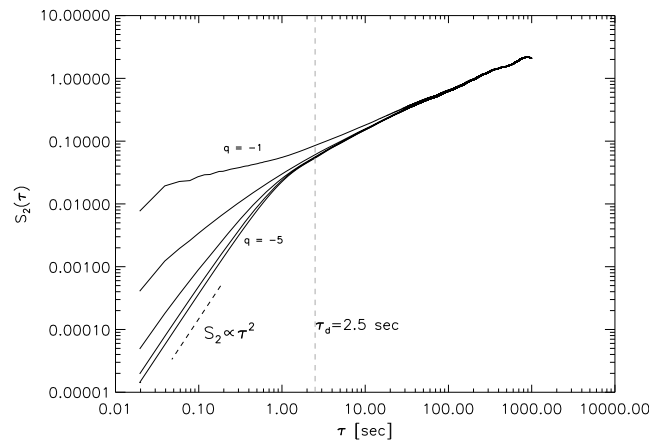


**Figure 2.** The structure function computed from the time series data for a number of values of  $q$ . The bottom curve is associated with a  $q$  value of  $-5$ , and the higher curves are determined with  $q = -4, -3, -2,$  and  $-1$ , respectively.

relevant to solar wind observations. For scales smaller than ion inertial length, the solar wind spectral slope is found to be quite variable. For example, *Smith et al.* [2006b] estimate that dissipation range magnetic spectral indices are broadly distributed with average values  $|q| = 2.61 \pm 0.96$  for intervals lacking magnetic clouds, and  $|q| = 2.01 \pm 0.84$  for cloud intervals.

A lesson can be learned from the above simple exercise: the asymptotic form of the correlation function embodied in equations (3) and (8) is not obtained until the sampled spectrum is  $k^{-4}$  or steeper. Between spectral indices  $-4$  and  $-3$ , the transition to the asymptotic parabolic form migrates toward finer scales, until at  $k^{-3}$ , the transition is delayed until separations within the assumed inner cutoff scale are sampled.

From equation (8), we can compute the correlation function from the structure function. Figure 3 displays the correlation function for various  $q$ . From these plots, we can see that the correlation function has a parabolic shape at the origin. At this fixed resolution, the characteristic parabolic shape becomes better defined as the values of  $|q|$  are increased.

Suppose now we select a known  $q$  and we compute the radius of curvature of the correlation function from data over a range of small separations near the origin  $0 < \tau \leq \tau_{\text{fit}}$ . While this value is intended to be small, to attempt to capture the parabolic regime (if present), the specific value  $\tau_{\text{fit}}$  has no physical significance—it is just a maximum lag to be used in a fitting procedure. This choice of a range of data provides an estimate of  $\tau_{\text{TS}}$ ; let us call it  $\tau_{\text{TS}}^{\text{est}}(\tau_{\text{fit}})$ . At this point we have obtained an approximate fit, or representation, of the data in this range of  $\tau$ , given by

$$\hat{R}(\tau) = 1 - \frac{\tau^2}{2 [\tau_{\text{TS}}^{\text{est}}(\tau_{\text{fit}})]^2}. \quad (9)$$

This fit is inexact even if the measurements are perfect, because we expect that the Taylor scale is  $\tau_{\text{TS}} = \lim_{\tau_{\text{fit}} \rightarrow 0} \tau_{\text{TS}}^{\text{est}}(\tau_{\text{fit}})$ . It is not practical to compute this limit because the data has finite time resolution  $\Delta t$  and because there may be limited data available at the shortest time lags. In another section below we will systematically examine the influence of  $\Delta t$ , the data sampling time.

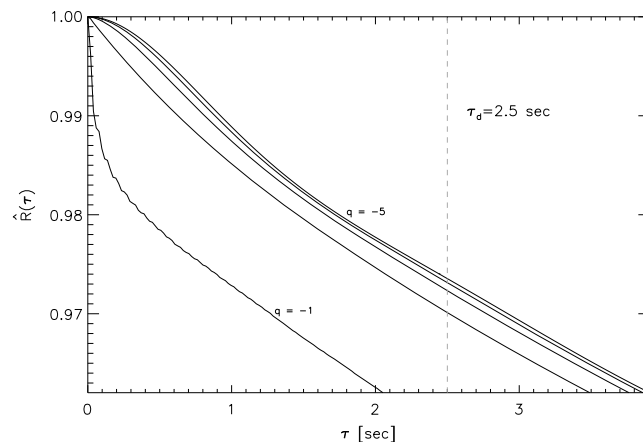


**Figure 3.** The correlation function near the origin. The top curve is determined from  $q = -5$  and the next curves are calculated using  $q = -4, -3, -2,$  and  $-1$ , respectively.

This is the regime, in accordance with equation (8), in which parabolic curvature of the correlation function is seen near  $\tau = 0$ .

- For  $\tau \ll \tau_d$ , but  $q$  values of  $-3$  or shallower, the required parabolic behavior is not seen near  $\tau_d$ , but rather this asymptotic behavior is deferred until  $\tau < 1/f_e$ . This is due to the fact that the spectrum for this range of  $q$  is not steep enough to cause convergence of the Taylor scale estimate. This convergence is now delayed until scales are sampled that are finer than the electron dissipation scale.

This change in behavior of Taylor scale estimates as the dissipation range spectral index is varied and is actually very

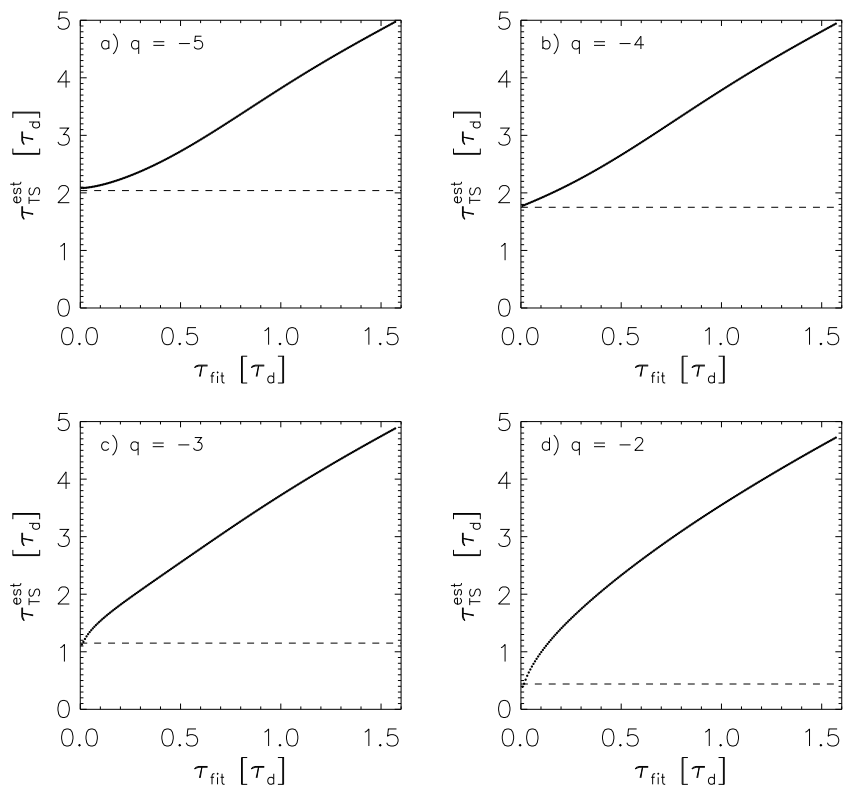


**Figure 4.** Taylor microscale from parabolic fit of the correlation function near the origin for each  $\tau_{\text{fit}}$  for a number values of  $q$ . Axes are in units of  $\tau_d$ . Dashed line indicates the exact Taylor microscale.

What can be done, however, is to compute  $\tau_{\text{TS}}^{\text{est}}(\tau_{\text{fit}})$  for a range of  $\tau_{\text{fit}}$  and to examine the trend of the corresponding values of  $\tau_{\text{TS}}^{\text{est}}$  as the maximum lag used in the fit becomes smaller. Figure 4 illustrates sequences of such fits  $\tau_{\text{TS}}^{\text{est}}(\tau_{\text{fit}})$  versus  $\tau_{\text{fit}}$ . Each of these curves approaches the exact value of Taylor scale in the limit of zero  $\tau_{\text{fit}}$ , as expected. This is for an idealized model times series that can be evaluated at any time separation we wish. Consequently, when a range of  $\tau_{\text{TS}}^{\text{est}}$  is available, but only for a set of values of  $\tau_{\text{fit}}$  that excludes the origin, one can try to recover a more precise value of  $\tau_{\text{TS}}$  by an extrapolation technique that provides a refined estimate of the radius of curvature at the origin.

## 2.2. Extrapolation Method

To obtain a stable value for the Taylor microscale at  $\tau = 0$ , we apply a method based on the Richardson extrapolation technique [see *Dahlquist and Bjorck*, 2003] in analogy with similar procedures employed in numerical analysis. In the first step we compute a series of parabolic fits to data near the origin, and for varying values of  $\tau_{\text{fit}}$ , up to a largest values of  $\tau_{\text{fit}}$ , say,  $\tau_{\text{max}}$ . Using the available estimated values of Taylor microscale  $\tau_{\text{TS}}^{\text{est}}(\tau_{\text{max}})$  for this range of  $\tau_{\text{max}}$ , we can compute a straight line extrapolation of the Taylor scale back to the origin ( $\tau_{\text{fit}} = 0$ ). This extrapolation gives a single estimate of a refined value of the Taylor microscale.

Still, it remains unclear which value of  $\tau_{\text{max}}$  we should use. On the one hand, a larger  $\tau_{\text{max}}$  permits the use of more data in the fit process, but a smaller  $\tau_{\text{max}}$  moves us closer to the asymptotic range in which the formula equation (9) for approximating the radius of curvature at the origin becomes more exact. Therefore, we will look for a stable range of values, as follows.

Figure 5 illustrates the variation of the extrapolated values of Taylor microscale as the value of  $\tau_{\text{max}}$  is varied. In the next step of the method we examine whether for some range of  $\tau_{\text{max}}$  we find a stable value of estimated  $\tau_{\text{TS}}^{\text{est}}$ . When working with real data with time cadence  $\Delta t$ , this process is constrained by the temporal resolution, i.e.,  $\tau_{\text{fit}} > \Delta t$ . The distribution of number of available estimates at each lag  $\tau$  can also become an issue. In addition, the quality of the refinement of the Taylor microscale value will depend on the steepness of the spectrum (i.e.,  $q$ ) at the high frequencies.

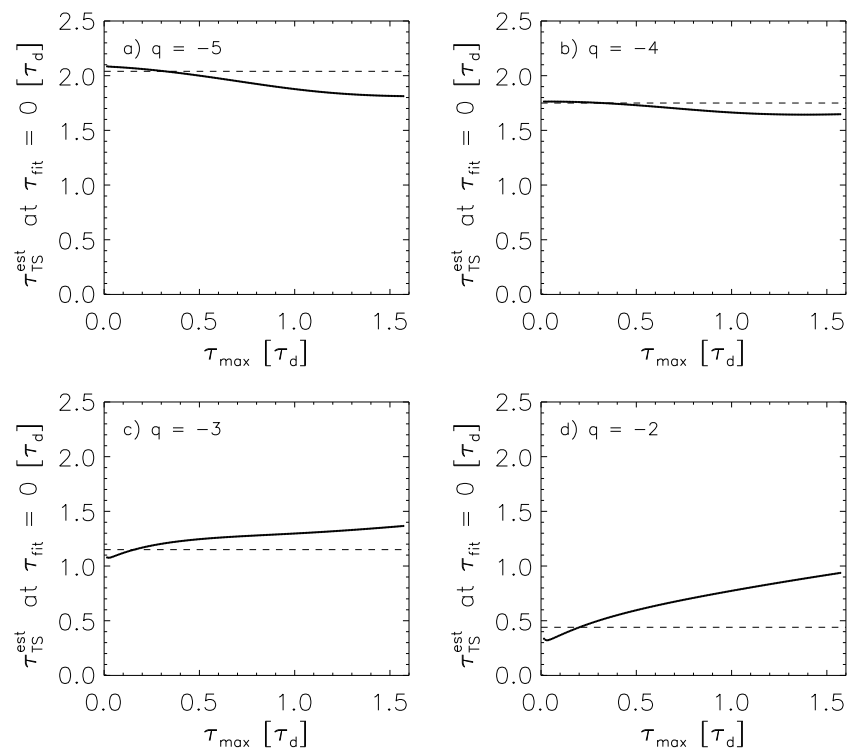


**Figure 5.** Values of  $\tau_{TS}$  determined by linear extrapolation from the data in Figure 4 at the origin (i.e., the intercept). Plotted are the extrapolated Taylor microscale values determined from a range of  $\tau_{max}$ .

In the next section we will discuss more details regarding the effects of data resolution and  $q$ . For now, (see Figure 5) we can make some general statements regarding quality of estimation when a range of estimates is available for time lags near the dissipation (spectral steepening) scale. For large values of  $|q|$ , where the correlation function has a large radius of curvature at the origin (compared to  $\tau_d$ ), we find a stable value of the Taylor microscale as  $\tau_{max}$  approaches zero. In contrast, for small values of  $|q|$ , we do not obtain a stable value of  $\tau_{TS}$  after the extrapolation.

One can also see by examining Figure 5 how lower time resolution data can have an adverse effect. Larger  $\Delta t$  means that the data close to the origin become unavailable for the extrapolation near  $\tau_{fit} = 0$ . The best we might be able to do in such cases is to choose a stable value in the range of  $\tau_{max}$  to  $\tau_d$ . By trying this out with the graphs, we see that this approach yields an underestimate of the Taylor microscale value when  $|q|$  is approximately greater than 4 and an overestimate when  $|q|$  is approximately less than 4. Our results suggest that a good estimate of  $\tau_{TS}$  is obtained by a linear extrapolation to zero lag using the slope of the curves  $\tau_{TS}^{est}(\tau_{fit})$  evaluated near  $\tau_{max} = \tau_d$  (see Figure 4). In the next subsection we will discuss how we can further improve this estimate with a correction ratio that takes into account known information about the spectra at higher frequencies.

### 2.3. Correction Ratio

The resolution of the observational data is limited by the instrumentation, the spacecraft data downlink, and spacecraft data storage. The lower resolution of the data is the less accurate the Taylor microscale value will be, since the measurements become less sensitive to the radius of curvature of the correlation function at the origin. In this section, we examine the effect of the temporal resolution of the data by artificially reducing the resolution of the synthetic time series and again estimating the Taylor microscale with the same method. The new values for each resolution of the data can be compared with the expected Taylor microscale value to assess the impact of the temporal resolution. In particular, the ratio  $\tau_{TS}^{expect} / \tau_{TS}^{est}$  is of interest. We call this ratio a “correction factor” as it can be employed to estimate the actual Taylor scale given the value computed from finite time resolution data. However, this correction must assume knowledge of the spectra at unresolved frequencies. Here that amounts to knowledge of the value of  $q$ .

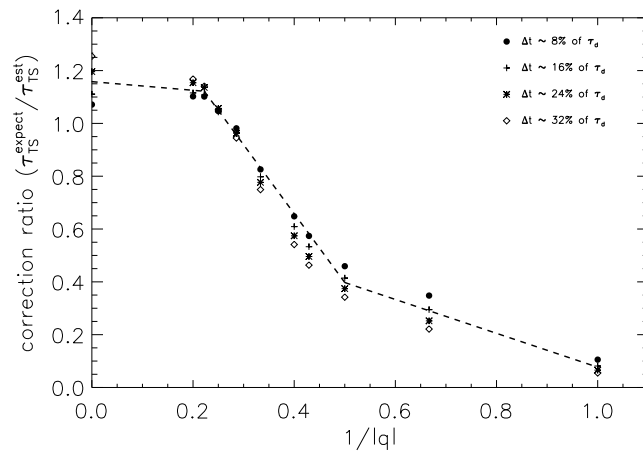


Figure 6 demonstrates the variation of the correction factor when we vary the temporal resolution  $\Delta t$  and the spectral index  $|q|$ . We can see that the correction ratio strongly depends on  $|q|$ . There are three regimes of behavior apparent in the figure, which we approximate as a piecewise linear function. The model suggests a correction for the Taylor scale estimates obtained from finite time resolution data. Accordingly, the empirical correction factor  $r(|q|)$  can be written as

Figure 6. Correction ratio versus  $1/q$  for number of different  $\Delta t$  values.

$$r(|q|) = \begin{cases} -0.64 \left( \frac{1}{|q|} \right) + 0.72, & \text{when } |q| < 2 \\ -2.61 \left( \frac{1}{|q|} \right) + 1.70, & \text{when } 2 \leq |q| < 4.5 \\ -0.16 \left( \frac{1}{|q|} \right) + 1.16, & \text{when } |q| \geq 4.5. \end{cases} \quad (10)$$

With this model for a given data set and a known value of  $q$ , it is possible to compute a corrected value of the Taylor microscale using

$$\tau_{TS} \approx r(|q|)\tau_{TS}^{extra} \quad (11)$$

where  $\tau_{TS}^{extra}$  is an estimate obtained by the extrapolation method described in section 2.2 above. This procedure presupposes that sufficient data are available to approximately determine the asymptotic tendencies of the correlations. From a practical perspective this appears to require that information about the functions near the dissipation scale  $\tau_d$  be included in the analysis. Based on the present numerical experiments, we recommend therefore that the resolution of the data be at least as good as  $\Delta t < 0.4\tau_d$ .

### 3. Applying the Technique to Spacecraft Data

From an analysis of the magnetic field data from the ACE spacecraft [Smith *et al.*, 2006a], the Taylor microscales in the left column of Figure 7 are determined by employing the extrapolation method described above but without applying the correction ratio. We use the same data set of ACE observations as was employed by Smith *et al.* [2006a, 2006b] and Hamilton *et al.* [2008]. The time resolution of the ACE data used here is  $\delta t = 0.333$  s or three vectors per second. The analysis of the ACE proceeds in the following way: The second-order structure function matrix is computed for each interval in the set of intervals studied. The Taylor scale is then estimated using a series of maximum lag approximations from a maximum lag of four data points to a maximum lag of 25. A line is fit to these estimated values of the Taylor scale as a function of maximum lag, and the lag = 0 intercept is computed. This gives the final estimated values shown in the figure. The dissipation scale is computed from the power spectrum as the intercept between two fit lines, one describing the ion inertial range frequencies and the other describing the ion dissipation range frequencies. The dissipation range spectral index  $q$  is determined from the short wavelength fit.

The black color shows the data from regions characterized as open magnetic field line regions, and the red color shows the data from magnetic clouds (closed field regions). The Taylor scales have already been converted to spatial scales by using the frozen-in approximation.

The values obtained for dissipation range spectral index lie between  $-5$  and  $-1$ , and the ratio of Taylor scale ( $\lambda_T$ ) to the dissipation scale ( $\lambda_d$ ) ranges between 0.1 and 10. The individual plots show that the red and black



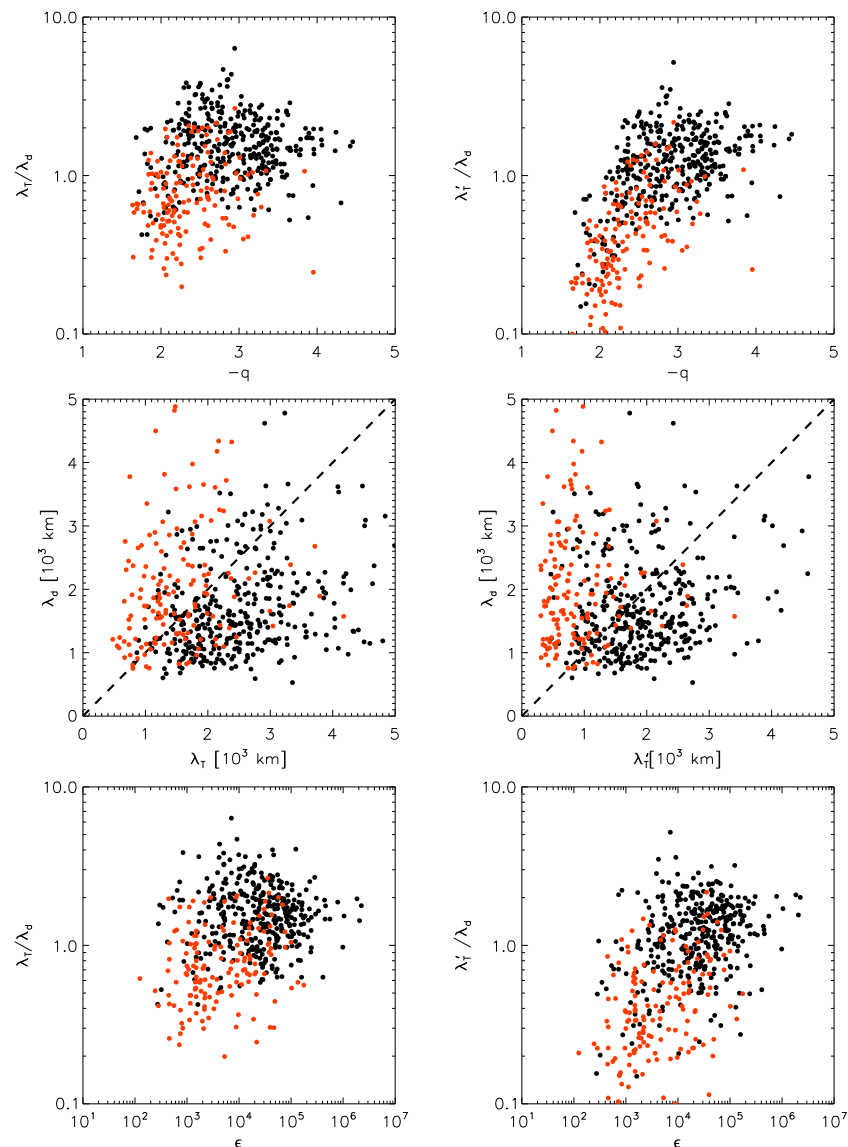


**Figure 7.** The left column shows the plots before applying the correction ratio to the Taylor microscale  $\lambda_T$ , and the right column shows the Taylor microscale ( $\lambda'_T$ ) after applying correction ratio.

points appear to be equally scattered. The right column of Figure 7 shows the values of  $\lambda'_T$ , after the application of the correction ratio. After the corrections, we can see that the majority of the black points have  $\lambda'_T > \lambda_d$  for  $q < -3$ , and the red points have  $\lambda'_T < \lambda_d$  for  $q > -3$ . This indicates a hydrodynamics type of plasma for open magnetic field case and nonhydrodynamics in the magnetic cloud cases. Further discussion of this analysis is found in *Matthaeus et al. [2008]*, where it is argued that the difference in the behavior of these cases points to a difference in relative importance of dissipative processes at ion and electron scales.

#### 4. Conclusions

We have demonstrated a refined technique of calculating the Taylor microscale from a discrete times series by computing correlation functions from structure functions. The method that we employed is based on the definition of the Taylor microscale. To verify this technique we analyze a synthetic time series derived from a defined power density spectrum. We are able to reproduce the Taylor scale values with our technique after applying a correction term, which improves our estimate of the Taylor microscale, estimated from a Richardson extrapolation technique [see *Weygand et al., 2009*]. In addition, we studied the effects of the dissipation range spectral index and the time resolution of the simulated data. Moreover, we show an example of the

application of the technique to solar wind magnetic field data [Matthaeus *et al.*, 2005, 2008]. This technique is expected to be useful for extracting refined estimates of the Taylor microscale from experimental and observational turbulence data in solar wind and other astrophysical contexts.

#### Acknowledgments

P. Chuychai was supported by Thailand Research Fund and Thailand's Commission on Higher Education, Ministry of Education (MRG 5286239). J.M. Weygand was partially supported by NSF SHINE: NSF AGS-1155841 and NASA Heliophysics Guest Investigator program NNX09AG31G. W.H. Matthaeus was partially supported by NSF SHINE AGS-1156094 and NASA under the Heliospheric GI program NNX09AG31G and the Solar Probe Plus project and the Magnetosphere Multiscale project. C.W. Smith is supported by the Advanced Composition Explorer mission. S.D. acknowledges partial support by the Argentinean grant UBACYT 20020120100220 (UBA).

Philippa Browning thanks D. Roberts and an anonymous reviewer for their assistance in evaluating this paper.

#### References

- Alexandrova, O., J. Saur, C. Lacombe, A. Mangeney, J. Mitchell, S. J. Schwartz, and P. Robert (2009), Universality of solar-wind turbulent spectrum from MHD to electron scales, *Phys. Rev. Lett.*, *103*, 165,003.
- Batchelor, G. K. (1970), *Theory of Homogeneous Turbulence*, Cambridge Univ. Press, Cambridge, U. K.
- Dahlquist, G., and A. Björck (2003), *Numerical Methods*, Courier Dover Publications, Mineola, New York, Prentice-Hall 1974.
- Dasso, S., W. H. Matthaeus, J. M. Weygand, P. Chuychai, L. J. Milano, C. W. Smith, and M. G. Kivelson (2008), ACE/Wind multispacecraft analysis of the magnetic correlation in the solar wind, in *Proceedings of the 30th International Cosmic Ray Conference. July 3–11, 2007, Mérida, Yucatán, Mexico*, vol. 1, edited by R. Caballero *et al.*, pp. 625–628, Universidad Nacional Autónoma de México, Mexico City, Mexico.
- Gary, S. P., and J. E. Borovsky (2004), Alfvén-cyclotron fluctuations: Linear Vlasov theory, *J. Geophys. Res.*, *109*, 6105, doi:10.1029/2004JA010399.
- Gurgiolo, C., M. L. Goldstein, W. H. Matthaeus, A. Vinas, and A. N. Fazakerley (2013), Characteristics of the Taylor microscale in the solar wind/foreshock: Magnetic field and electron velocity measurements, *Ann. Geophys.*, *31*, 2063, doi:10.5194/angeo-31-2063-2013.
- Hamilton, K., C. W. Smith, B. J. Vasquez, and R. J. Leamon (2008), Anisotropies and helicities in the solar wind inertial and dissipation ranges at 1 AU, *J. Geophys. Res.*, *113*, A01106, doi:10.1029/2007JA012559.
- Hinze, J. O. (1975), *Turbulence*, McGraw-Hill, New York.
- Leamon, R. J., W. H. Matthaeus, and C. W. Smith (1998), Contribution of cyclotron-resonant damping to kinetic dissipation of interplanetary turbulence, *Astrophys. J.*, *507*, L181, doi:10.1086/311698.
- Matthaeus, W. H., and M. L. Goldstein (1982), Stationarity of magnetohydrodynamic fluctuations in the solar wind, *J. Geophys. Res.*, *87*, 10,347–10,354.
- Matthaeus, W. H., S. Dasso, J. M. Weygand, L. J. Milano, C. W. Smith, and M. G. Kivelson (2005), Spatial correlation of solar-wind turbulence from two-point measurements, *Phys. Rev. Lett.*, *95*, 231,101, doi:10.1103/PhysRevLett.95.231101.
- Matthaeus, W. H., J. M. Weygand, P. Chuychai, S. Dasso, C. W. Smith, and M. Kivelson (2008), Interplanetary magnetic Taylor microscale and implications for plasma dissipation, *Astrophys. J.*, *678*, L141, doi:10.1086/588525.
- Sahraoui, F., M. L. Goldstein, P. Robert, and Y. V. Khotyaintsev (2009), Evidence of a cascade and dissipation of solar-wind turbulence at the electron gyroscale, *Phys. Rev. Lett.*, *102*, 231,102, doi:10.1103/PhysRevLett.102.231102.
- Smith, C. W., K. Hamilton, J. Vasquez, and R. J. Leamon (2006a), Dependence of the dissipation range spectrum of interplanetary magnetic fluctuations on the rate of energy cascade, *Astrophys. J.*, *645*, L85, doi:10.1086/506151.
- Smith, C. W., B. J. Vasquez, and K. Hamilton (2006b), Interplanetary magnetic fluctuation anisotropy in the inertial range, *J. Geophys. Res.*, *111*, A09111, doi:10.1029/2006JA011651.
- Taylor, G. I. (1938), The spectrum of turbulence, *Proc. R. Soc. London, Ser. A*, *164*, 476–490.
- Weygand, J. M., W. H. Matthaeus, S. Dasso, M. G. Kivelson, and R. J. Walker (2007), Taylor scale and effective magnetic Reynolds number determination from plasma sheet and solar wind magnetic field fluctuations, *J. Geophys. Res.*, *112*, A10201, doi:10.1029/2007JA012486.
- Weygand, J. M., W. H. Matthaeus, S. Dasso, M. G. Kivelson, L. M. Kristler, and C. Mouikis (2009), Anisotropy of the Taylor scale and the correlation scale in plasma sheet and solar wind magnetic field fluctuations, *J. Geophys. Res.*, *114*, A07213, doi:10.1029/2008JA013766.
- Weygand, J. M., W. H. Matthaeus, M. El-Alaoui, S. Dasso, and M. G. Kivelson (2010), Anisotropy of the Taylor scale and the correlation scale in plasma sheet magnetic field fluctuations as a function of auroral electrojet activity, *J. Geophys. Res.*, *115*, A12250, doi:10.1029/2010JA015499.
- Weygand, J. M., W. H. Matthaeus, S. Dasso, and M. G. Kivelson (2011), Correlation and Taylor scale variability in the interplanetary magnetic field fluctuations as a function of solar wind speed, *J. Geophys. Res.*, *116*, A08102, doi:10.1029/2011JA016621.